THE ASTROPHYSICAL JOURNAL, 566:L71–L75, 2002 February 20

AVERAGE QUASAR SPECTRA IN THE CONTEXT OF EIGENVECTOR 1[1]

J. W. SULENTIC,[2] P. MARZIANI,[3] R. ZAMANOV,[3] R. BACHEV,[2,3] M. CALVANI,[3] AND D. DULTZIN-HACYAN[4]

Received 2001 November 24; accepted 2002 January 11; published 2002 January 22

ABSTRACT

Recent work has shown that it is possible to systematize quasar spectral diversity in a parameter space called "Eigenvector 1" (E1). We present median active galactic nucleus (AGN) spectra for fixed regions of the E1 (optical) parameter space [FWHM(Hβ) vs. equivalent width ratio $R_{\rm Fe\,II} = W({\rm Fe\ II}\ \lambda4570)/W({\rm H}\beta)$]. Comparison of the median spectra shows considerable differences. We suggest that an E1-driven approach to median/average spectra emphasizes significant differences between AGNs and offers more insights into AGN physics than a single-population median/average spectrum derived from a large and heterogeneous sample of sources. We find that the Hβ broad component line profile changes along the E1 sequence in FWHM, centroid shift, and profile asymmetry. While objects with FWHM($H\beta_{\rm BC}$) $\lesssim$ 4000 km s^{-1} are well fitted by a Lorentz function, AGNs with FWHM($H\beta_{\rm BC}$) $\gtrsim$ 4000 km s^{-1} are better fitted if two broad-line components are used: a "classical" broad-line component and a very broad/redshifted component.

Subject headings: galaxies: active — quasars: emission lines — quasars: general

On-line material: color figures

1. INTRODUCTION

Studies of broad emission line spectra for active galactic nuclei (AGNs) provide the strongest constraint on models for the nebular physics and on kinematic models of the broad-line–emitting clouds. Ideally, one would like to have both high signal-to-noise ratio (S/N) and moderate-resolution ($\lesssim$5 Å) measures for the strongest high- and low-ionization lines as well as measures across as wide a wavelength range as possible in order to better characterize the continuum shape. Measures of this kind have led to the Eigenvector 1 (E1) parameter space concept (Sulentic, Marziani, & Dultzin-Hacyan 2000a; Sulentic et al. 2000c) that is, in part, built on foundations laid 10 years ago (Boroson & Green 1992). The above spectroscopic requirements are very observing time intensive, but recent AGN surveys have provided an alternate method for examining quasar spectra at very high S/N. Average or composite spectra derived from large survey databases involving hundreds of AGNs (the Large Bright Quasar Survey: Francis et al. 1991; the *Hubble Space Telescope* Faint Object Spectrograph database: Zheng et al. 1997; the FIRST Bright Quasar Survey: Brotherton et al. 2001; the Sloan Digital Sky Survey: Vanden Berk et al. 2001) make it possible to generate a "typical" quasar spectrum from blueward of Lyα to Hα.

What is unclear is whether such composite spectra are astrophysically useful beyond, perhaps, allowing us to identify lines that are too weak to be seen in individual source spectra. The fundamental question is whether the similarities or the differences in AGN line and continuum phenomenology tell us more about the underlying physics. The E1 concept has been advanced as a possible "H-R diagram" for AGNs in the sense that it appears to provide parameter-space discrimination between all major classes of broad-line sources as well as a correlation for, at least, radio-quiet sources (Sulentic et al. 2000c). The correlation and distribution of radio-quiet sources [with FWHM(Hβ) $\leq$ 4000 km s^{-1}] in E1 have been reasonably well fitted with a model that sees the accretion rate, convolved with source orientation, as the principal physical driver (Marziani et al. 2001). The generality of E1, of course, requires much further testing, but unless it is far off the mark, it suggests that indiscriminate average or composite spectra should be viewed in the same way that one would view an average stellar spectrum taken over the full effective temperature range that is observed in the H-R diagram (spectral types O–M). Interpretation of composite spectra from heterogeneous samples will be complicated in two ways: (1) they will be subject to selection biases dependent on the relative number of sources with each "spectra type" in a given sample, and, more significantly, (2) they will average the spectra of sources with dramatically different broad-line spectral characteristics. We suggest that the most useful approach to averaging AGN spectra lies within the E1 context. We present average spectra for fixed domain quadrants in E1 followed by a brief discussion of important differences. The emphasis is on the FWHM(Hβ) measures, although large differences in the $R_{\rm Fe\,II}$ parameter are also seen. A full discussion of the equivalent width measures must wait for significant numbers of very high S/N spectra of Fe II$_{\rm opt}$ weak sources.

2. SAMPLE, DATA REDUCTION, AND ANALYSIS

Our current sample includes optical spectra for 187 sources that were obtained between 1988 and 1996. They cover the wavelength range that includes Hγ, Hβ, and most of the optical Fe II emission (4200–5700 Å in the rest frame). Spectra were obtained with the following telescopes and spectrographs: ESO 1.5 m (Boller & Chivens [B&Ch]), San Pedro Martir 2.2 m (B&Ch), Calar Alto 2.2 m (B&Ch), KPNO 2.2 m (Gold), and Mount Ekar (Asiago) 1.82 m (B&Ch). Data for 52 objects can be found in Marziani et al. (1996), and the unpublished part of the data set will appear in a forthcoming paper (P. Marziani et al. 2002, in preparation). Spectra were taken with very similar instrumental setups, including typically a 120 Å mm^{-1} dispersion and a 2″ slit width yielding resolution in the range of 4–7 Å FWHM. The S/N is typically in the range of ≈20–30. Spectra with S/N $\lesssim$ 10 were excluded. The sample includes spectra for 187 type 1 AGNs with redshifts $z \lesssim 0.8$ and apparent magne-

[1] Based in part on data collected at the ESO, La Silla.

[2] Department of Physics and Astronomy, University of Alabama at Tuscaloosa, Box 870324, Tuscaloosa, AL 35487-0324.

[3] Osservatorio Astronomico di Padova, Vicolo dell'Osservatorio 5, I-35122 Padova, Italy.

[4] Instituto de Astronomía, UNAM, Apdo Postal 70-264, 04510 Mexico DF, Mexico.

TABLE 1
SAMPLE PROPERTIES

Type	$R_{\rm Fe\,II}$	FWHM($H\beta_{\rm BC}$) (km s^{-1})	$N_{\rm obj}$	$N_{\rm RL}$	M_B[a]	σ_{M_B}	$\overline{\rm FWHM(H\beta_{BC})}$[b] (km s^{-1})	$\overline{R_{\rm Fe\,II}}$	$\overline{c(1/2)}$[b, c] (km s^{-1})	$\overline{c(1/4)}$[b, c] (km s^{-1})	Best Fit
Total	All	All	187	64	−23.7	2.0	...	0.37	...	...	...
NLSy1	All	≤2000	24	2	−23.0	1.7	1500	0.61	40	0	Lorentz
Population A[d]	All	≤4000	80	11	−23.3	1.8	2300	0.49	20	30	Lorentz
A3	1.0–1.5	0–4000	5	0	−24.5	2.2	2350	1.23	−280	−290	Lorentz
A2	0.5–1.0	0–4000	26	3	23.3	1.5	1950	0.70	−20	−30	Lorentz
A1	0.0–0.5	0–4000	49	6	−23.2	1.8	2250	0.31	30	250	Lorentz
Population B[e]	All	>4000	97	50	−24.2	2.0	5700	0.22	200	700	Double-Gaussian
B1	0.0–0.5	4000–8000	76	35	−24.2	2.0	5600	0.23	250	700	Double-Gaussian
B1^{+}	0.0–0.5	8000–12000	17	12	−24.1	2.1	10000	0.17	270	1700	Double-Gaussian
B1^{++}	0.0–0.5	>12000	4	3	...	...	...	...	...	...	...
Outliers	>0.5	>4000	10	3	−23.0	2.3	...	0.80	...	...	...

[a] Absolute B magnitude from the Véron-Cetty et al. (2001) catalog for $H_0 = 50$ km s^{-1} Mpc^{-1} and $q_0 = 0$.
[b] Values measured on a high-order spline function representative of the $H\beta_{\rm BC}$ of each median spectrum.
[c] Centroids at fractional intensity are defined as $c(i/4) = (\lambda_B + \lambda_R - 2\lambda_0)/\lambda_0$, where $\lambda_0 = 4861.33$ Å and λ_B and λ_R are the wavelengths of the blue- and red-line side at the given fractional intensity, respectively.
[d] Population A ≡ A1 ∪ A2 ∪ A3.
[e] Population B ≡ B1 ∪ B1^{+} ∪ B1^{++}, with outliers (O) excluded.

tudes $m_V \lesssim 17.0$. Table 1 summarizes the properties of our data sample (see § 3.1 for bin definition). Composite spectra were obtained by taking the median of all spectra with 1 Å resolution. The S/N of the composite spectra was ≳100, except for bin A3 where only five objects were available and S/N ≈ 50. No composite spectra were obtained for the rare objects in the outlier domain [FWHM($H\beta_{\rm BC}$) ≳ 4000 km s^{-1} and $R_{\rm Fe\,II} \gtrsim 0.5$] that spans several E1 bins.

The following analysis procedures were applied to each spectrum (see Marziani et al. 1996 for details): (1) deredshifting using the narrow-line component of Hβ and/or [O III] λ4959, 5007 as rest-frame measures; (2) normalization using the best estimate for a local continuum at λ ≈ 5100 Å; (3) subtraction of Fe II λ4570 emission blends using a template based on the spectrum of I Zw 1 that also yielded the Fe II blend equivalent width W(Fe II λ4570); (4) subtraction of the [O III] λ4959, 5007 and He II λ4686 lines; and (5) subtraction of the narrow component from Hβ (H$\beta_{\rm NC}$) using a Gaussian model. In cases for which no clear inflection between broad and narrow components was seen, two alternative approaches were employed: (1) we assumed that FWHM(H$\beta_{\rm NC}$) ≈ FWHM([O III] λ5007), or (2) we assumed that FWHM(H$\beta_{\rm BC}$) ≈ FWHM(Fe II λ4570). The latter approach was useful for narrow-line Seyfert 1 (NLSy1) sources. Following these procedures, we extracted H$\beta_{\rm BC}$ and derived equivalent width and FWHM measures that allowed us to populate E1. Host galaxy contamination was not significant for the luminous AGNs included in this sample. The typical uncertainty for FWHM(H$\beta_{\rm BC}$) is about 10%, and for W(H$\beta_{\rm BC}$) and W(Fe II λ4570) about 10%–15%. Errors on $R_{\rm Fe\,II}$ are estimated to be less than 0.2.

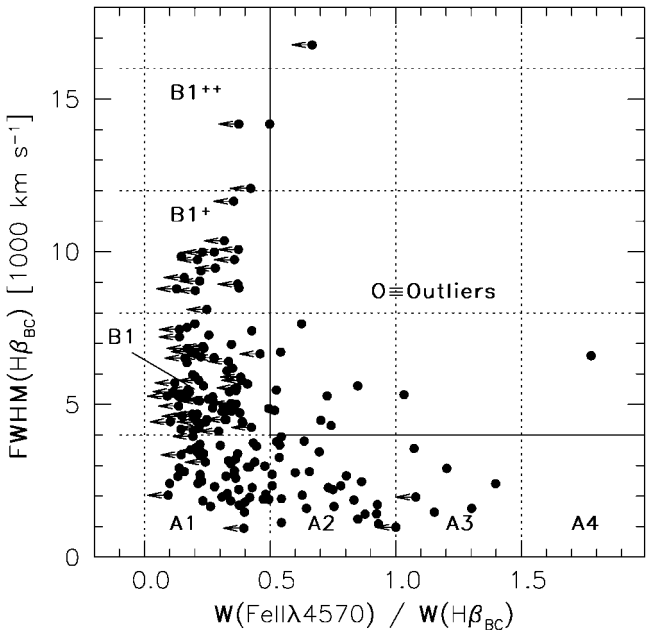

FIG. 1.—Optical parameter plane of E1. This is the largest sample yet displayed in an E1 context. The dotted lines indicate the adopted binning of the optical E1 plane, while the solid lines separate the region of maximum source occupation from the outlier zone that is, so far, largely a zone of avoidance in quasar parameter space. The abscissa is $R_{\rm Fe\,II} = W$(Fe II λ4570)/W(H$\beta_{\rm BC}$). Horizontal arrows denote Fe II λ4570 upper limits. Note that upper limits dominate single $R_{\rm Fe\,II}$ measurements in the B1 and B1^{+} domains, while the higher S/N of the median spectra allow for a more accurate determination. [*See the electronic edition of the Journal for a color version of this figure.*]

3. RESULTS

3.1. *Spectral Types*

The distribution of 187 sources in the optical E1 plane [FWHM(H$\beta_{\rm BC}$) vs. $R_{\rm Fe\,II}$] is shown in Figure 1. We binned the optical parameter plane as shown in Figure 1 and as defined in Table 1. The bins were arbitrarily set to constant ΔFWHM(H$\beta_{\rm BC}$) = 4000 km s^{-1} and $\Delta R_{\rm Fe\,II} = 0.5$. A finer subdivision is not warranted at this time by the accuracy of the measures or the heterogeneity of the data sample. The adopted A–B bin labeling reflects our earlier suggestion that two distinct radio-quiet AGN populations may exist: population A ("pure" radio-quiet) and population B (same as the radio-loud domain; see Table 1). The numeral accompanying the letter designation for A bins reflects the increasing strength of $R_{\rm Fe\,II}$. The "+" designations for B bins reflect increasing FWHM(H$\beta_{\rm BC}$). There are many measures that distinguish between radio-quiet population A and B as defined with a boundary at FWHM(H$\beta_{\rm BC}$) ≈ 4000 km s^{-1}. There are also many measures that support a phenomenological commonality between population B and radio-loud sources (Sulentic et al. 2000a, 2000b, 2000c). Table 1 summarizes the properties of domain space bins that are occupied by a significant number of sources. The composite (median) spectra after processing step 2 (continuum-normalized) and after step 3 (Fe II$_{\rm opt}$ subtracted) are

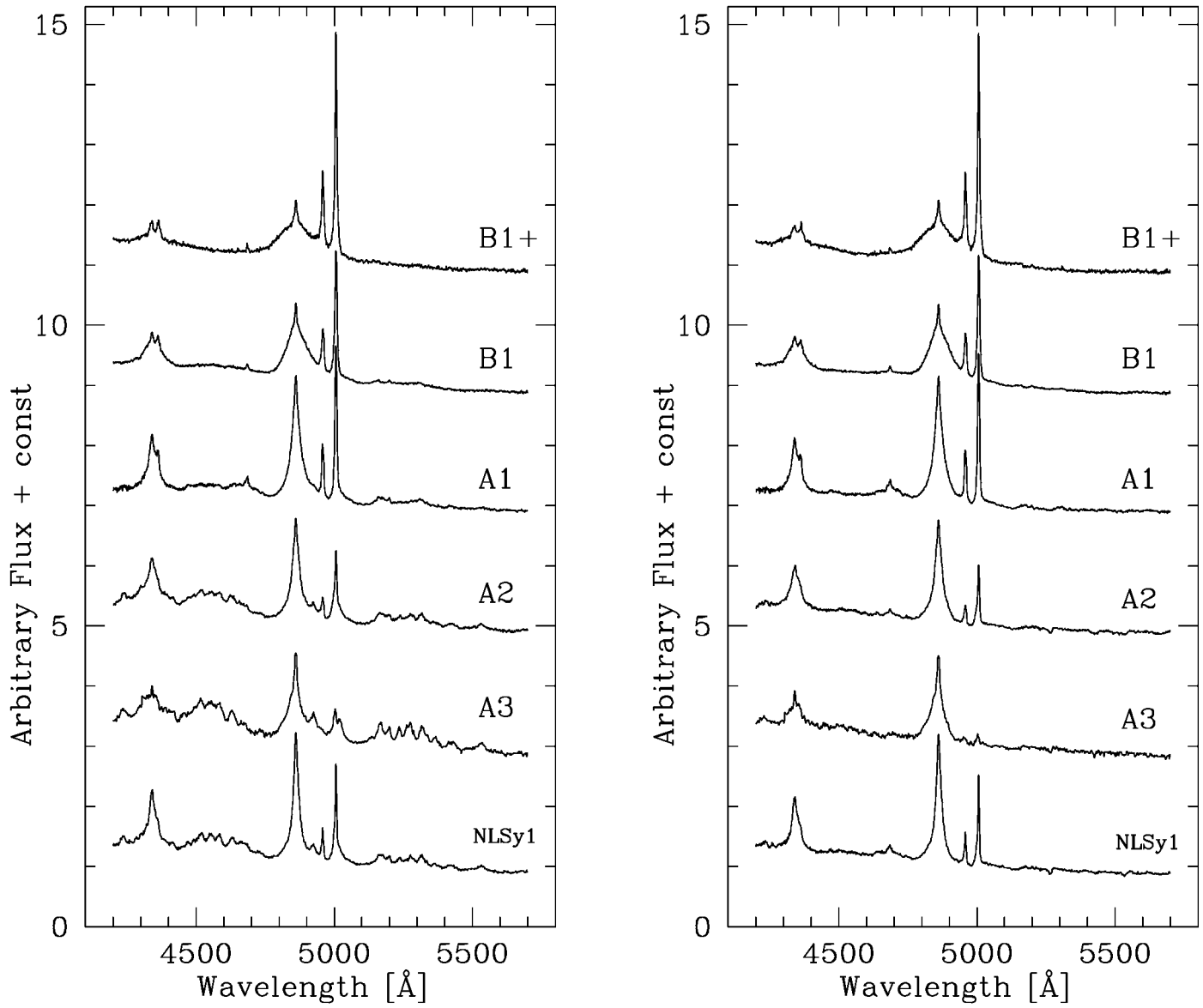

FIG. 2.—*Left panel*: Composite (median) spectra of the E1 parameter bins defined in Table 1 and Fig. 1. *Right panel*: Same composite spectra with Fe II$_{opt}$ emission subtracted.

presented in the left and right panels of Figure 2, respectively. The median spectra are available in digital format on the World Wide Web.[5]

It is important to note that the E1-binned median spectra are unlikely to be strongly influenced by any luminosity dependence since there is, so far, no convincing evidence for a difference in line profile properties with source redshift/luminosity (Sulentic et al. 2000a) and for any subsample, $\Delta M_B \lesssim 1.5 \lesssim \sigma_{M_B}$ (see Table 1). It is also worth noting that the median M_B of our sources is close to the limit separating Seyfert 1 galaxies and quasars ($M_B = -23.0$). This should not be considered a particular problem because there is no discontinuity in the AGN luminosity distribution. Radio-loud sources in our sample show a higher mean luminosity, perhaps due to the inclusion of many beamed sources. At the same time, population B radio-quiet sources, cospatial with them in E1, are not more luminous than population A radio-quiet sources.

[5] At the address http://panoramix.pd.astro.it/~marziani/medians.zip.

Our W(Fe II λ4570) uncertainty estimate (§ 2) is valid if Fe II λ4570 is clearly detected above the noise. However, the minimum W(Fe II λ4570) for which it is possible to visually detect Fe II λ4570 depends both on the S/N and on the Fe II λ4570 FWHM. For S/N ≈ 20, upper limits for Fe II λ4570 detection is estimated to be ≈14, 17, and 20 Å for FWHM = 2500, 5000, and 7500 km s^{-1}, respectively. The utility of the composite spectra is also evident because of the much higher S/Ns in bins B1 and B1$^+$, which contain many upper limits because Fe II λ4570 is intrinsically weak in population B sources. In those bins, it is possible to obtain more reliable W(Fe II λ4570) measurements from composite spectra.

3.2. *Median* Hβ_{BC} *Profiles across E1*

Median spectra of the Hβ_{BC} profile are shown in Figure 3. They were extracted from the median spectra after Fe II$_{opt}$ and continuum subtraction to take advantage of the much higher S/N of the compositer spectra. We derived a pure Hβ_{BC} profile

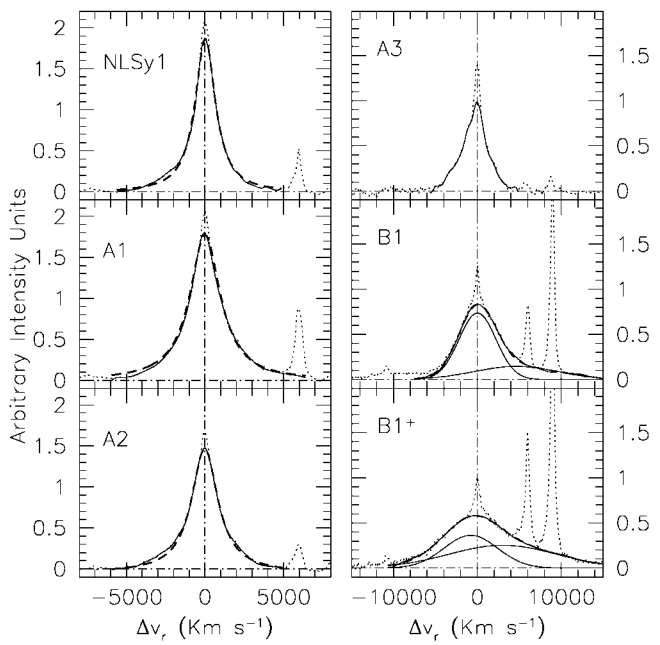

FIG. 3.—Continuum-subtracted Hβ composite line profiles for the different E1 parameter bins defined in Fig. 1. The solid lines show the profile H$\beta_{\rm BC}$ after subtraction of narrow-line emission components. A Lorenztian fit (*dashed line*) is superposed on the NLSy1, A1, and A2 profiles. The individual components of a double-Gaussian (*thin lines*) and resultant fit (*dashed line*) are shown for B1 and B1$^+$. [*See the electronic edition of the Journal for a color version of this figure.*]

by first subtracting [O III] λ4959, 5007 and He II λ4686 and then fitting H$\beta_{\rm BC}$ with a high-order spline function to avoid the effects of a finite S/N and to interpolate across the H$\beta_{\rm NC}$. This approach has proven to be successful for measuring line parameters in noisier line profiles (Marziani et al. 1996). It is preferable to template fitting because it makes no assumptions about the shape of the profile. Table 1 presents FWHM(H$\beta_{\rm BC}$) as well as line centroids at $\frac{1}{2}$ and $\frac{1}{4}$ maximum intensities derived from the median spectra. The median H$\beta_{\rm BC}$ profiles in population A are almost symmetric, with a slight blueward asymmetry in bin A2. The blue asymmetry becomes visually apparent in bin A3, which contains sources that are extreme in many ways. Table 1 shows that the profiles of NLSy1 sources do not differ from bin A1 and A2 median spectra. The smaller median FWHM H$\beta_{\rm BC}$ reflects an arbitrary cutoff ($\leq$2000 km s^{-1}) in the definition of NLSy1 sources.

The profiles of population A sources are very different from those of population B. The median profiles of population B sources are very red asymmetric, with the strongest asymmetry in the (few) bin B1^{++} sources. The different shape may point toward different broad-line region (BLR) structure/kinematics in these sources. The profile shape was not selected a priori in the population definition that was based on a possible FWHM(H$\beta_{\rm BC}$) break. An alternate way to describe profile asymmetry involves fitting a functional form to the median profiles. The H$\beta_{\rm BC}$ profile in NLSy1 sources is well fitted by a Lorentz function (see also Véron-Cetty, Véron, & Gonçalves 2001). The same is generally true for A1 and A2 median profiles, while A3 is based on only five sources.

A Lorentz function is definitely not a satisfactory description for bin B median profiles. The H$\beta_{\rm BC}$ profile is significantly different, and this can be seen even in Figure 2. The profile becomes more Gaussian, but we were unable to fit bin B profiles with any simple and physically meaningful function. The best fits to H$\beta_{\rm BC}$ bin B1 and B1$^+$ profiles required the sum of two Gaussians: (1) *a* FWHM $\approx$ 4000–5000 km s^{-1} *unshifted Gaussian core and* (2) *a broader* FWHM $\approx$ 10,000 km s^{-1} *redshifted* ($\Delta v_r \sim$ 5000 km s^{-1}) *Gaussian base*. The main difference between B1 and B1$^+$ may be related to the strength of the "very broad component." We will show in the next section that many radio-loud and some radio-quiet population B sources show unambiguous, very broad components and that the interpretation of the profile in terms of two components may have a straightforward physical meaning.

4. DISCUSSION

We find significant and systematic differences in median spectra across E1. FWHM(H$\beta_{\rm BC}$) and $R_{\rm Fe\,II}$ both show systematic changes, and the other E1 parameters reinforce this dichotomy (population A sources show a systematic blueshift of the C IV λ1549 broad-line profile and a soft X-ray excess while population B source do not; Sulentic 2000a, 2000c). Population A sources show a more symmetric profile with the largest $R_{\rm Fe\,II}$-values [indicating large W(Fe II λ4570) and somewhat depressed W(H$\beta_{\rm BC}$)]. As one enters the population B domain, the radio-loud source fraction increases dramatically. H$\beta_{\rm BC}$ becomes increasingly broad and red asymmetric for both radio-loud and radio-quiet sources. Overall, NLSy1/population A sources show lower ionization than do population B (Marziani et al. 2001). Comparison between high (C IV λ1549$_{\rm BC}$; HIL) and low (H$\beta_{\rm BC}$; LIL) ionization emission lines suggests that they are emitted in disjoint regions in population A. Contrarily, both LIL and HIL may arise from a single region in population B sources (Marziani et al. 1996; Sulentic et al. 2000a, 2000c). It is more accurate to say that we cannot rule out the possibility that both HIL and LIL arise from the same line-emitting regions (broad and very broad) in population B (Sulentic et al. 2000a). The H$\beta_{\rm BC}$ profile analysis indicates that the BLR—and specifically the region emitting the low-ionization lines—is most probably structurally different in population A and population B sources. It is beyond the scope of the present Letter to report on a detailed model calculation. We note, however, that the Lorentz profile is consistent with emission from an extended accretion disk. This reinforces the suggestion that the LIL spectra in population A sources arise from a disk. The situation is less clear for population B sources, where the Eddington ratio may be much lower. There is good evidence that sometimes only one of the two emission components is present in population B sources (a pure BLR or a pure very broad line region [VBLR]; see Sulentic et al. 2000b). In a companion paper, we suggest that even the narrow-line region structure/kinematics may be changing along the E1 sequence (R. Zamanov et al. 2002, in preparation).

4.1. *The Very Broad Line Region Issue*

Can the double-Gaussian model that is needed to fit population B (and radio-loud) profiles be physically justified? Several lines of evidence point toward the existence of a VBLR at the inner edge of the BLR (Corbin 1997a, 1997b). Emission from this region may be thought of as a sort of inner large covering factor "boundary layer" where gas begins to become optically thick (Marziani & Sulentic 1993; Sulentic et al. 2000b). In objects like the luminous quasar PG 1416−129, almost pure VBLR emission survived after a continuum intensity decrease effectively quenched the classical BLR. 3C 232 (Marziani et al. 1996) may represent a good radio-loud analog of PG 1416. Other examples of possible pure VBLR

line sources can be found in Sulentic et al. (2000b). He II λ4686 has also been known for some time to show a profile systematically broader than Hβ in some sources (see Osterbrock & Shuder 1982), and this can be seen in Figure 2. Unfortunately, He II λ4686 is usually weak and/or blended with stronger Hβ and Fe II emission (it is on the red end of Fe II λ4570). Detection of the He II λ4686 broad component is therefore a function of the Fe II_{opt} strength and S/N. The strongest very broad He II λ4686 feature is seen in the bin A1 median spectrum, where we have a favorable combination of S/N, FWHM Hβ, Fe II_{opt} weakness, and He II λ4686 strength. The latter bias reflects the inclusion of data from an observing run dedicated to studying strong He II λ4686 emission. A very broad He II λ4686 profile is sometimes seen in population A sources (e.g., Ton S 180) with much narrower Fe II λ4570. However, in I Zw 1, the highest S/N spectra fail to show any trace of He II λ4686 emission. At this time, the question of He II λ4686 emission must be considered on an object-by-object basis. We note that the He II λ4686 strength was an orthogonal (Eigenvector 2) parameter in the principal component analysis of Boroson & Green (1992).

5. CONCLUSION

We generated average QSO spectra in the 4200–5700 Å spectral region for fixed optical parameter bins in E1. In such bins, the mean spectral type appears to change systematically across E1. This systematic behavior is also reflected in E1 X-ray and UV measures. Composite spectra in an E1 context should provide useful input for theoretical modeling. Ignoring the diversity of the AGN $H\beta_{BC}$ profile may make any theoretical modeling of the BLR kinematics and dynamics unreliable.

The authors acknowledge support from the Italian Ministry of University and Scientific and Technological Research (MURST) through grant and Cofin 00-02-004.

REFERENCES

Boroson, T. A., & Green, R. F. 1992, ApJS, 80, 109
Brotherton, M. S., Tran, H. D., Becker, R. H., Gregg, M. D., Laurent-Muehleisen, S. A., & White, R. L. 2001, ApJ, 546, 775
Corbin, M. R. 1997a, ApJS, 113, 245
———. 1997b, ApJ, 485, 517
Francis, P. J., Hewett, P. C., Foltz, C. B., Chaffee, F. H., Weymann, R. J., & Morris, S. L. 1991, ApJ, 373, 465
Marziani, P., & Sulentic, J. W. 1993, ApJ, 409, 612
Marziani, P., Sulentic, J. W., Dultzin-Hacyan, D., Calvani, M., & Moles, M. 1996, ApJS, 104, 37
Marziani, P., Sulentic, J. W., Zwitter, T., Dultzin-Hacyan, D., & Calvani, M. 2001, ApJ, 558, 553
Osterbrock, D. E., & Shuder, J. M. 1982, ApJS, 49, 149
Sulentic, J. W., Marziani, P., & Dultzin-Hacyan, D. 2000a, ARA&A, 38, 521
Sulentic, J. W., Marziani, P., Zwitter, T., Dultzin-Hacyan, D., & Calvani, M. 2000b, ApJ, 545, L15
Sulentic, J. W., Zwitter, T., Marziani, P., & Dultzin-Hacyan, D. 2000c, ApJ, 536, L5
Vanden Berk, D. E., et al. 2001, preprint (astro-ph/0105231)
Véron-Cetty, M.-P., Véron, P., & Gonçalves, A. C. 2001, A&A, 372, 730
Zheng, W., Kriss, G. A., Telfer, R. C., Grimes, J. P., & Davidsen, A. F. 1997, ApJ, 475, 469 (erratum 492, 855 [1998])